Thermal behavior of materials in laser-assisted extreme manufacturing: Raman-based novel characterization

OPEN ACCESS
IOP Publishing | IMMT
International Journal of Extreme Manufacturing
Int. J. Extrem. Manuf. **2** (2020) 032004 (17pp)
https://doi.org/10.1088/2631-7990/aba17c

Topical Review

Thermal behavior of materials in laser-assisted extreme manufacturing: Raman-based novel characterization

Ridong Wang[1,5], Shen Xu[2,5], Yanan Yue[3,5] and Xinwei Wang[4]

[1] State Key Laboratory of Precision Measuring Technology and Instruments, Tianjin University, Tianjin 300072, People's Republic of China
[2] School of Mechanical and Automotive Engineering, Shanghai University of Engineering Science, Shanghai 201620, People's Republic of China
[3] School of Power and Mechanical Engineering, Wuhan University, Wuhan 430072, People's Republic of China
[4] Department of Mechanical Engineering, Iowa State University, Ames, IA 50011, United States of America

E-mail: xwang3@iastate.edu

Received 10 March 2020, revised 8 April 2020
Accepted for publication 29 June 2020
Published 30 July 2020

Abstract

Laser-assisted manufacturing (LAM) is a technique that performs machining of materials using a laser heating process. During the process, temperatures can rise above over 2000 °C. As a result, it is crucial to explore the thermal behavior of materials under such high temperatures to understand the physics behind LAM and provide feedback for manufacturing optimization. Raman spectroscopy, which is widely used for structure characterization, can provide a novel way to measure temperature during LAM. In this review, we discuss the mechanism of Raman-based temperature probing, its calibration, and sources of uncertainty/error, and how to control them. We critically review the Raman-based temperature measurement considering the spatial resolution under near-field optical heating and surface structure-induced asymmetries. As another critical aspect of Raman-based temperature measurement, temporal resolution is also reviewed to cover various ways of realizing ultrafast thermal probing. We conclude with a detailed outlook on Raman-based temperature probing in LAM and issues that need special attention.

Keywords: Raman spectroscopy, temperature response, spatial resolution, temporal resolution, ultrafast characterization

(Some figures may appear in colour only in the online journal)

[5] These authors contributed equally to this work.

2631-7990/20/032004+17$33.00

1. Introduction

Laser-assisted manufacturing (LAM) is a method that applies the instantaneous heating capability of a laser with a focused beam to materials that are difficult to process by mechanical machining alone [1, 2]. This method has been applied in various manufacturing processes, including drilling, cutting, turning, peening, nanoimprinting, additive manufacturing, scanning probing microscope, etc [1, 3–10].

In the laser-assisted drilling (LAD) process, the laser beam is focused on the workpiece surface to melt or evaporate the material. An assisted gas is used to blow away the molten material or vapor. This technique is widely used in many areas, such as heavy machinery, aerospace, marine, chemical, and automotive industries, etc [5, 11]. Similar to LAD, in the laser-assisted cutting process, the laser beam is focused on the material, melting material around the focal point. The melted material is blown away by the assisting cutting gas. This method has applications in punching, cut-off, and marking of metals, ceramics, and plastics [12].

Laser-assisted turning, which combines turning and laser heating, is a suitable alternative to the grinding process of hard-to-manufacture materials. In this process, the laser is used to heat up a material in the cutting zone to reduce the material's strength. Thus, the cutting force can be significantly reduced, improving the material's machinability. This process can also increase productivity and accuracy, reduce installation spaces and energy consumption [1, 13].

Laser peening is an efficient thermo-mechanical approach to engineer and modify the surface and subsurface related properties of materials. It is widely used in aerospace, automotive, shipbuilding, biomedical, microelectronics, and microelectromechanical systems [7, 14]. This process uses a pulsed laser to irradiate the surface and generate a shock wave. The recoil pressure/stress wave in the substrate compresses and hardens the surface of the substrate [15–17].

Laser nanoimprinting is a technique that utilizes a laser pulse to irradiate the sample surface. The sample surface is in contact with and pre-loaded by a mold (e.g. fused quartz) with prefabricated nanoscale features on its contact side. Upon irradiating the laser pulse on the sample surface, the near-surface materials melt, forming a laser-induced molten layer, which allows the mold to impinge into the sample directly. The nano-patterns transform from the mold to the sample as the molten layer cools and solidifies [18, 19]. This technique has been used widely for making photonic bandgap crystals [20].

Laser additive manufacturing has attracted significant attention in recent years. It is a technology that uses material accumulation to produce solid parts. The machining process is based on the CAD digital model to stratify the data of the material model, and then layer by layer to generate three-dimensional entities by laser processing. The two most common techniques of this technology are selective laser melting and laser cladding deposition. In both techniques, the metal powder is melted by the laser to form the desired entity [21]. Laser additive manufacturing has been widely used in aerospace, medical, automotive, electronics, and military fields [21–25].

In laser-assisted scanning probing microscope (SPM, e.g. scanning tunneling microscope and atomic force microscope) surface nanostructuring, a laser irradiates the tip surface, forming near-field focusing on an extremely small region (i.e. a few nm). The tip undergoes a thermal expansion upon pulsed laser irradiation, resulting in mechanical contact with the sample surface to form nano-indentation [26–28]. The tip could also act as a receiving antenna that collects laser energy and as a transmitting antenna to the tip to enhance the optical field by a few orders of magnitude. The enhanced optical field can heat the sample surface to induce phase change or chemical reaction and modify the surface at the nanoscale [26, 29, 30].

All the above outlined processes involve intensive heating, which indicates that the heating level/material's thermal response is critical for understanding the physics behind the laser-assisted manufacturing, and for providing feedback for manufacturing optimization. The infrared thermometry technique is widely used for temperature measurement [31–33]. It measures the infrared thermal radiation from the heating region (if the temperature is very high, the measured radiation wavelength is visible). But it is difficult to measure the transient response of the sample, especially under ultrafast laser pulse heating or for regions that are too small to probe, such as those used in nanoscale/near-field manufacturing. A thermocouple-based technique can also be used to measure the temperature [31, 34–36]. The thermocouple is comprised of two dissimilar conductors to measure unknown temperature with reference to the known temperature. This contact technique has more limitations in terms of transient response, measurement capacity/range, and spatial resolution.

Raman spectroscopy, which is widely used for structure characterization, can also be used for temperature probing [37–41]. This technique provides a novel way to measuring temperature during laser-assisted extreme manufacturing and can provide unique and unprecedented knowledge about the physics involved in laser extreme manufacturing. The following sections present a comprehensive critical review about various Raman-based techniques that can be used for temperature probing.

2. Raman-based temperature probing

2.1. Mechanism of Raman scattering

In 1928, C V Raman discovered the inelastic scatterings of photons from matter when incident photons interacted with matter [42, 43]. These inelastic scatterings, termed Raman scatterings, originate from the change in polarizability of vibrational modes of chemical bonds in molecules, which is the instant deformity of the electric dipole of molecules due to the incidence of an electromagnetic field [44, 45]. The electric dipole moment μ is proportional to the incident electric field with a polarizability a, and has an expression as following [45]:

$$\mu = a_0 E_0 \cos\omega_0 t + \frac{1}{2}\left(\frac{\partial\alpha}{\partial q}\right)\Big|_{q=0} \cdot q_0 E_0 \cos(\omega_0 - \omega_R)\, t + \frac{1}{2}\left(\frac{\partial\alpha}{\partial q}\right)\Big|_{q=0} \times q_0 E_0 \cos(\omega_0 + \omega_R)\, t, \tag{1}$$

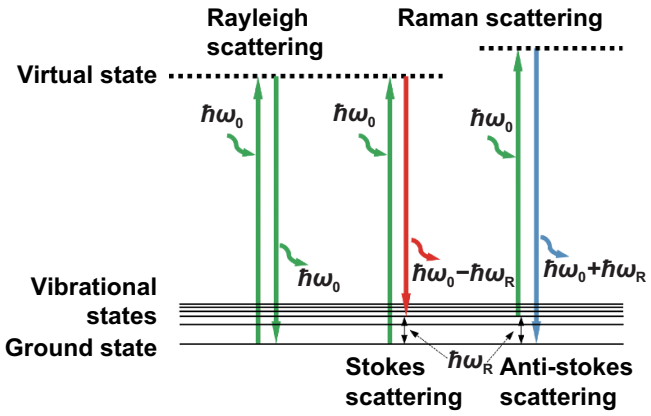

Figure 1. The mechanism of Stokes and anti-Stokes scatterings generation.

where E_0 is the incident electric field, ω_0 and ω_R are the frequencies of the incident photons and vibrational mode, a_0 is the original polarizability, and q is the nuclear motion. On the right side in equation (1), the first term stands for Rayleigh scatterings, the second term is for Stokes scatterings, and the third term is anti-Stokes scatterings, as shown in figure 1.

The Stokes scatterings arise when the chemical bonds absorb the incident photon energy ($h\omega_0$), the electrons are excited to a virtual state, then de-excited to an excited state, and emit new photons with a lower energy ($h\omega_0 - h\omega_R$) [46]. Different from the Stokes scattering, anti-Stokes scatterings occur when electrons in an excited state are excited to the virtual state, then return to the ground state and emit photons. The scattered photons gain energy from the molecules and have a higher energy than the incident photons as ($h\omega_0 + h\omega_R$) [47]. The amount of energy gained or lost by the vibrational modes ($h\omega_R$) depends on its nucleus mass and the strength of the chemical bonds involved in the Raman scattering. Therefore, the frequency shift (ω_R) of Raman scatterings, either Stokes or anti-Stokes, is uniquely related to a specific chemical bond, and the corresponding Raman spectrum is considered to be a material's chemical 'fingerprint'. Since Raman scatterings respond to the change in vibrational modes of chemical bonds, they vary as vibrational modes change under different environmental factors, such as temperature and stress. Therefore, changes in Raman spectra can be used to measure temperature, which is termed Raman thermometry [48].

2.2. Raman-based temperature probing

Temperature variation of the tested sample affects the properties of its Raman peaks, when other measuring conditions are well controlled. Take a Stokes Raman peak as an example: when the temperature increases, its Raman wave number red shifts, intensity decreases, and linewidth broadens [49–51]. In a certain temperature range of approximately 50° of variation [52, 53], the changing rates/temperature coefficients of these three properties could be safely assumed constant. Thus, the temperature can be determined based on a linear relation.

2.2.1. Temperature response of Raman peaks. Raman shift is the mostly commonly used property for temperature measurement in Raman thermometry. It originates from dipoles in the chemical bonds of materials. Its value directly indicates the specific structure of a material. Considering the fact that temperature increases affect the energy and thus the frequency of the vibrational mode, Raman shift responds to temperature. Raman shift moves to a lower value, or red shifts, as temperature goes higher; while it moves to a higher value, or blue shifts, when temperature decreases. Variation of Raman shift against temperature for Stokes peaks has the following expression [54]:

$$\omega(T) = \omega_0 + A\left(1 + \frac{2}{e^{\frac{h\omega_0}{4\pi kT}} - 1}\right) + B\left(1 + \frac{3}{e^{\frac{h\omega_0}{4\pi kT}} - 1} + \frac{3}{\left(e^{\frac{h\omega_0}{4\pi kT}} - 1\right)^2}\right), \tag{2}$$

where h and k are Planck's constant and Boltzmann's constant, T is the absolute temperature, A and B are constants specific to materials. Besides temperature, stress also affects the exact value of Raman shift because the stress-induced strain alters the bond force and the energy and frequency of the vibrational mode. In laser-assisted extreme manufacturing, a significant temperature rise occurs in the irradiated area, resulting in a very large temperature gradient around the laser spot. An accompanying high thermal stress may induce a corresponding Raman shift in addition to the temperature-induced shift. In this case, the stress-induced Raman shift should be carefully evaluated when determining temperature using Raman shift.

The Raman linewidth is an alternative parameter to determine the temperature in the case of high stress, for it depends on the lifetime of optical phonons in materials and is much less affected by stress. It is reported that temperature rise is accompanied by a decrease in phonon lifetime and thus a broadening in Raman linewidth. The mathematical expression of the Raman linewidth Γ against temperature is [54]:

$$\Gamma(T) = C\left(1 + \frac{2}{e^{\frac{h\omega_0}{4\pi kT}} - 1}\right) + D\left(1 + \frac{3}{e^{\frac{h\omega_0}{4\pi kT}} - 1} + \frac{3}{\left(e^{\frac{h\omega_0}{4\pi kT}} - 1\right)^2}\right). \tag{3}$$

C and D are the constants depending on materials. Though the linewidth is exclusively dependent on temperature, it is less sensitive to temperature change compared with Raman shift. It could serve as a suitable temperature indicator when Raman scatterings are sound enough to be well fitted using a Gaussian/Lorentzian shape.

The intensity of Raman scatterings, both Stokes and anti-Stokes, depend on the populations of their initial states. According to the principle of thermodynamic equilibrium, Stokes scatterings from a lower initial state have a larger population than that of anti-Stokes scatterings from an upper state. Thus, Stocks scatterings are much stronger than anti-Stokes in the spectrum. Both vary along with temperature. The ratio of

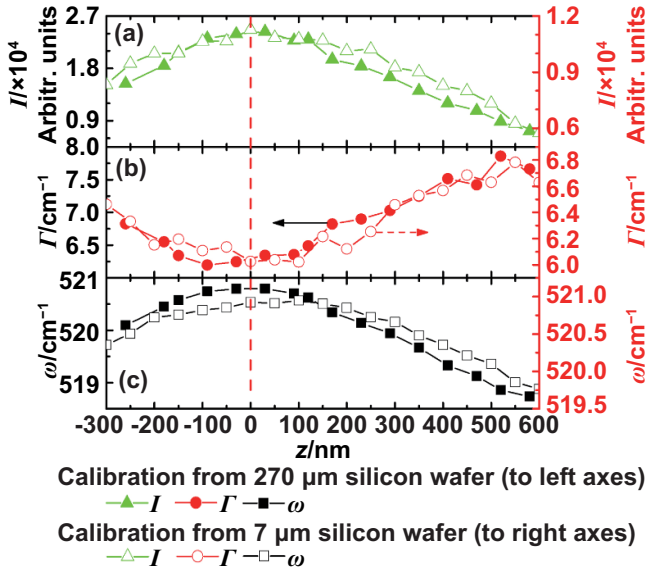

Figure 2. Out-of-focus effect induced variations in the intrinsic properties of the 521 cm^{-1} peak of silicon. Red dash line crossing $z = 0$ denotes the focal plane. (a) Raman intensity (I), (b) Raman linewidth (Γ), and (c) Raman shift (ω) for the 521 cm^{-1} peak. Reprinted from [55], Copyright (2017), with permission from Elsevier.

Stokes to anti-Stokes could directly reveal the absolute temperature of the sample [54].

$$\frac{I_s}{I_{as}} = \frac{\alpha_0 + \alpha_s}{\alpha_0 + \alpha_{as}} \left(\frac{\omega_0 - \omega_R}{\omega_0 + \omega_R} \right)^4 \exp\left(\frac{h\omega_R}{2\pi kT} \right), \quad (4)$$

where α_0, α_s, α_{as} are the absorbance regarding the incident photon frequency, Stokes frequency and anti-Stokes frequency, respectively. However, the Stokes and anti-Stokes peaks are rarely exhibited in one spectrum simultaneously based on current spectroscopy techniques. Researchers use the Stokes scatterings more often than the ratio of the intensity to measure temperature.

2.2.2. Optical focusing and out-of-focus effect on temperature measurement. Due to the fact that Raman scatterings are much weaker than Rayleigh scattering, around 10^{-8}, a focusing system and a long integration time are employed to increase the efficiency of Raman scattering acquisition [55]. However, these operations bring up another important issue: out-of-focus effect due to stage drift, that should be carefully addressed before temperature measurement. Xu *et al* studied the out-of-focus effect on Raman spectra using commercial silicon wafers with thicknesses of 270 μm and 7 μm, respectively, under a 100× microscope objective [56]. The silicon wafer was manually moved away from the focused level to obtain Raman spectra at different z positions. Figure 2 shows the variation of Raman properties of silicon's 521 cm^{-1} peak against the z position.

Figure 2 shows that Raman intensity is decreasing, Raman shift is red-shifting, and linewidth is broadening as the sample surface leaves the focal plane until the out-of-focus effect could be directly observed as blur images through the imaging system by the naked eye. It has a similar trend as Raman peaks varies along with temperature elevation and may cause errors in temperature measurement. Taking the Raman shift as an example, the out-of-focus effect induced a shift of 0.1 cm^{-1} when the surface moved away 90 nm from the focal level. This shift of 0.1 cm^{-1} is equivalent to a 7° rise in the temperature of silicon, based on the temperature coefficient of 0.015 cm^{-1} K^{-1} in previous work [54]. Thus, in Raman thermometry, maintaining the sample's surface at a well-focused level plays an extremely important role in measurement accuracy.

In previous work, thermal expansion was identified as one of the main reasons for the unexpected shift of the sample surface away from the focal plane. There are two contributing factors for thermal expansion: the sample and the sample stage [57, 58]. When the heating laser is focused on the sample surface and heats the sample up, the sample expands in both vertical and horizontal directions, and the sample's surface moves away from the focal plane. Thermal expansion depends on the thickness and is $\Delta L = \alpha \cdot L \cdot \Delta T$, where α is the thermal expansion coefficient.

The thermal expansion coefficient of most materials is in the order of 10^{-6} K^{-1} [59]. For suspended film-like materials, such as suspended graphene and other 2D materials, it is safe to neglect the thermal expansion as the samples are just several nanometers thick. However, in laser-assisted extreme manufacturing, large temperature rises and thick materials may cause non-negligible thermal expansion and further cause the samples surface to drift out of the focal plane in the thickness direction. Thermal expansion due to elevated temperatures also affect the sample stage which holds the sample during the manufacturing process. Though the temperature rise in the stage will not be as high as that in the sample, the centimeter-thickness of the stage will raise a large thermal expansion in the stage which causes the sample moving out of focal plane. Researchers have made great efforts to keep the sample at the focal level and reduce the out-of-focus effect to the greatest extent by either monitoring samples simultaneously in an optical imaging system or developing self-focusing systems [60–62].

2.3. Unique advantage of Raman thermometry: material-specific

Raman spectroscopy records the Raman scatterings, which provide vibrational information about all the chemical bonds in the excited/irradiated area by the incident laser. The 'fingerprint' feature of Raman peaks exhibits all the peaks discretely in one spectrum since the Raman peak is narrow enough. This is an advantageous feature of Raman thermometry because it can simultaneously distinguish all materials in the irradiated area and measure each material's temperature, as long as their scatterings are detectable. Along with the wide application of heterogeneous structure, Raman thermometry has been widely used to measure the temperature and thermophysical properties of multiple materials involved. Taking supported 2D materials as an example, it could probe the temperatures

of both the 2D materials and the substrate [63]. Raman thermometry can even measure Raman scattering in laser assisted nanostructures even though the parts are smaller than the incident laser spot. It can detect the chemical process of precursors and measure their temperatures in laser-assisted manufacturing, such as laser-assisted chemical vapor deposition and additive manufacturing [64, 65], to better monitor the manufacturing process and optimize the structure.

As the Raman excitation laser penetrates into part of the tested sample in the thickness direction, Raman scatterings are generated not only from the surface but also in the volume across the thickness. Therefore, the measured temperature based on Raman thermometry is an intensity-weighted temperature over the volume, specifically, over the depth of the irradiated area [61, 66]. The penetration depth τ depends on the wavelength of the incident laser λ and the extinction coefficient k of the material as $\tau = \lambda/4\pi k$. The penetration depth of silicon is calculated to be 820 nm under the excitation of 532 nm laser at room temperature. Additionally, the Raman scatterings in the irradiated area are not evenly distributed because the optical intensity of the incident laser has a Gaussian profile in the irradiated area. Therefore, a Raman-intensity weighted average temperature, $\Delta\bar{T} = \iiint \Delta T I_{Raman} dV / \iiint I_{Raman} dV$, has been proposed to fully consider this volume effect.

2.4. Calibration and its uncertainty

2.4.1. Case-based calibration. In Raman based temperature measurements, calibration is needed to know the temperature coefficient of Raman properties, like Raman shift, Raman intensity, and Raman linewidth. In a relatively narrow temperature range, the coefficients of the properties against temperature could be assumed to be linear based on previous research [52, 54]. A typical approach to calibrate these temperature coefficients is to place the sample on a heating stage which is precisely temperature-controlled by a thermal probe [49, 63, 66]. The temperature of the stage is then raised step by step and a corresponding Raman spectrum is recorded at each temperature step. By using Gaussian/Lorentzian function fitting, the exact values of each type of the Raman intrinsic properties are plotted against temperature to evaluate the slope of the linear curve, which is defined as the temperature coefficient for the Raman properties.

However, this calibration cannot be universal. Another calibration is required when the material structure varies or the measuring condition changes. For example, the temperature coefficient of graphene has been observed as a range of values (-0.015–0.076 $\mathrm{cm^{-1} \cdot K^{-1}}$) instead of a fixed value [67–69]. The structure of graphene samples, surrounding medium, and even the measurement condition leads to differences/errors in the calibrated temperature coefficients. The temperature coefficient of the Raman shift of the G peak was determined to be -0.016 $\mathrm{cm^{-1} \cdot K^{-1}}$ for a single-layered graphene and -0.015 $\mathrm{cm^{-1} \cdot K^{-1}}$ for a bi-layered sample [70]. The temperature coefficients of the Raman properties differ between suspended and supported graphene. The coefficient was reported to be -0.015 $\mathrm{cm^{-1} \cdot K^{-1}}$ for a suspended sample [71], -0.031 ± 0.005 $\mathrm{cm^{-1} \cdot K^{-1}}$ for a sample supported on a SiO_2 substrate [72], and -0.089 $\mathrm{cm^{-1} \cdot K^{-1}}$ for one supported on copper [73]. Furthermore, it has been reported that the temperature coefficient for the G peak differs under different wavelengths of excitation lasers [67–69, 74]. Therefore, it is necessary to conduct calibration for each sample in a defined Raman system. The experiment temperature range should be well covered in calibration.

2.4.2. Thermal expansion and stress effect in calibration. In addition to the sample's conditions, the process of Raman scattering acquisition inevitably introduces errors. As mentioned above, thermal expansions in both the sample and heating stage shift the sample's surface away from the focal level and cause extra errors due to the out-of-focus effect. These errors can be manually minimized by refocusing the sample. Other errors arise when the temperature rises in the collecting objective and its surrounding air. Heat automatically dissipates from the sample's surface to the cooler objective and surrounding air. This may account for variations in the temperature coefficient of the same sample. Wang's group calibrated the temperature coefficient of c-Si multiple times, and the reported value ranged from -0.019 to -0.0355 $\mathrm{cm^{-1} \cdot K^{-1}}$ in different works [60, 61, 66]. It is inevitable that the top layer (in a 2D material) and the local interface spacing could introduce some extra shift of the Raman wavenumber due to deflection of the back-scattered Raman beam. This may account for the widely scattered temperature coefficients of Raman wavenumber.

Moreover, different scenarios in the measurement and calibration also raise errors/deviations in temperature measurements, especially for layered materials. These factors were rarely considered until Tang *et al* discovered this phenomenon while studying the thermal behaviors of supported graphene [57, 58]. In the temperature measurement, the incident laser was focused on the sample's surface and heated the sample from the top. The focused heating spot raised the temperature gradient and generated thermal stress in the graphene layer. Moreover, the temperature increase in the graphene layer was higher than that in the substrate. This was due to two factors. One was the interface thermal resistance which partially impeded heat conduction through the interface. The other was that the substrate was a bulk that easily conducted heat and minimized heat accumulation and further temperature rise. Two materials thermally expanded differently, and due to the mismatch at the interface, the substrate built up another tensile stress in the graphene.

In contrast, both the graphene layer and substrate heated evenly on the heating stage during the calibration. The temperature also distributed uniformly in the graphene layer and no temperature gradient or thermal stress existed. Moreover, the graphene layer and substrate had the same temperature. Though there was still a thermal expansion mismatch, the mismatch-induced stress that the substrate places on the graphene was different from that in the interface characterization. This difference between the measurement and calibration could cause finite, yet nonnegligible errors in the determined temperature. Tang *et al* utilized the different

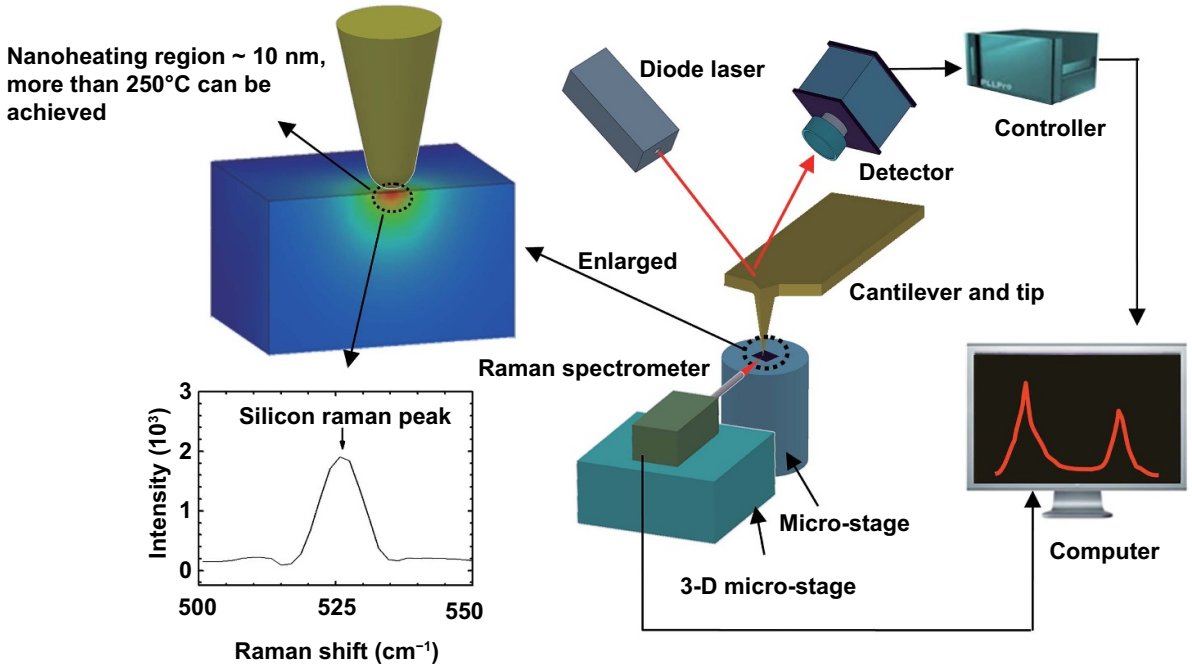

Figure 3. Experimental setup for tip-induced laser heating and temperature measurement based on Raman spectrum. Reprinted with permission from [75]. Copyright (2011) American Chemical Society.

sensitivities of Raman shift and linewidth in responding to stress and successfully deconjugated and quantified the temperature field and stress field, respectively [57, 58].

2.4.3. Additional consideration in laser extreme manufacturing. In the case of laser-assisted extreme manufacturing, a substantial temperature increase usually occurs in the irradiated area. Temperature determination based on the calibrated temperature coefficient cannot be satisfied. This is due to the fact that the temperature coefficient is regarded as a constant in a narrow temperature range within 50 K, but it becomes nonlinear in wider temperature ranges [52, 54]. The assumption of a constant temperature coefficient is not safe and may lead to errors in temperature determination. Besides, if the heated region shows high stress, either due to the large temperature gradient or the thermal expansion mismatch at interfaces, the stress will greatly affect the Raman shift. The heating during calibration is uniform, and no stress is involved [66]. Therefore, to consider the stress effect, it is essential to combine the Raman shift and linewidth when measuring temperature. This can also help determine the local stress.

Another commonly disregarded in Raman thermometry—which should be addressed in laser-assisted extreme manufacturing—is that the Raman intensity usually decreases as temperature increases. When temperature is very high, the Raman peaks become too weak to detect, not to mention temperature measurement based on the properties of Raman peaks. One way to overcome this problem is to employ resonance Raman spectroscopy to enhance the intensity of Raman scatterings in which the incident photon energy of the Raman excitation laser coincides with the energy of a selected electronic transition. The vibrational modes under this resonance electronic excitation show a 10^6- to 10^8-fold increment in polarizability and hence Raman intensity over spontaneous Raman [55]. It will help a great deal to achieve temperature measurement in the elevated temperature range in laser-assisted manufacturing.

3. Raman-based thermal probing in near-field laser manufacturing

In near-field laser manufacturing, the distance between the laser-focusing feature and the processed material is less than 10 nm. In addition, the laser focal spot is in the same order of size. Thus, it is very difficult to characterize the temperature and stress of the laser-heated material. Because the Raman signal is related to the temperature and structure of material, near-field Raman-based thermal probing, which is a non-contact technique with high resolution, can be used in such situations. Additionally, the Raman-uncovered temperature and stress field can be used to study the effect of various physical parameters, including laser power, polarization, wavelength, focal level, and pulse width. That is, the near-field Raman thermal probing technique holds promising potential for parameter optimization in near-field laser manufacturing.

3.1. Temperature response of the substrate under nano-tip near field heating

The near-field technology has been demonstrated to be very effective in laser-assisted manufacturing at extremely small

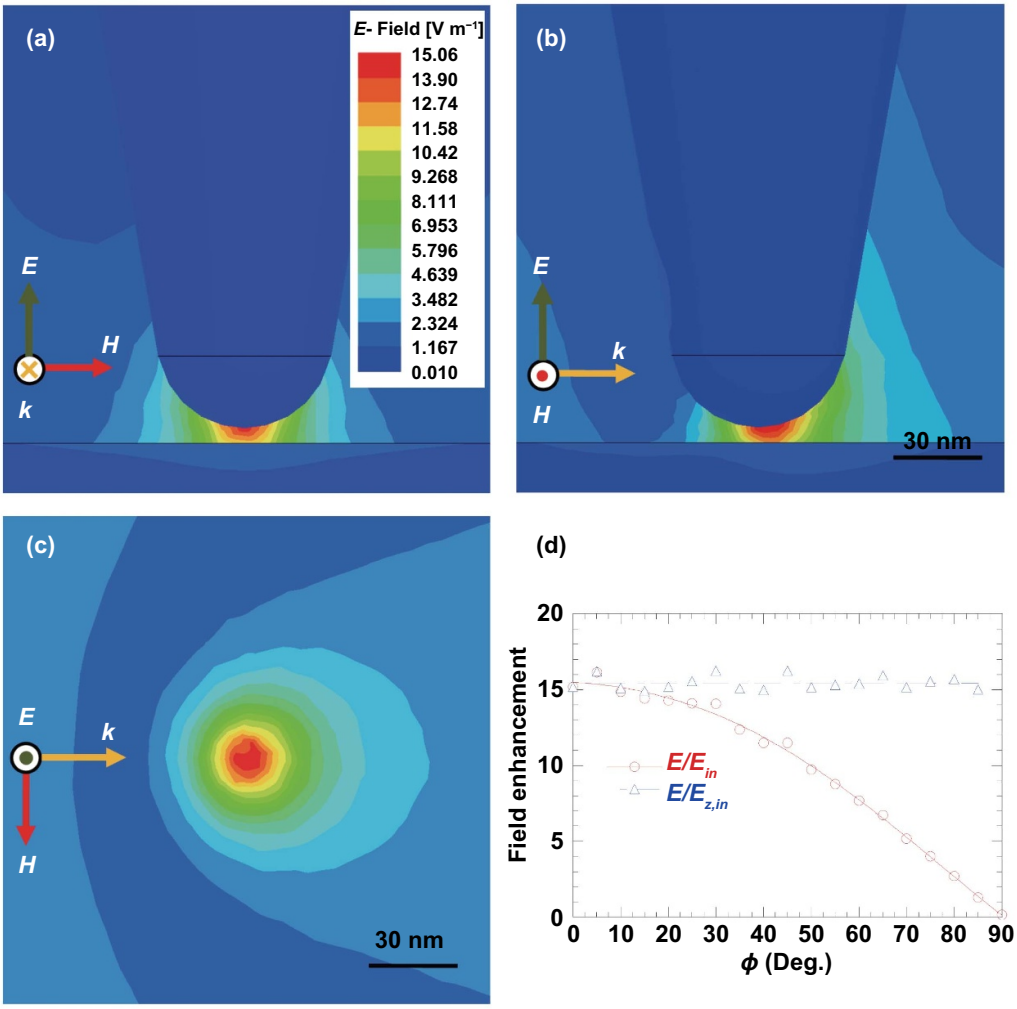

Figure 4. Electric field distribution around the tip apex for (a) the front view in the *y*–*z* plane, (b) the side view in the *x*–*z* plane, and (c) the top view of the cross-section under the tip apex; (d) field enhancement for different polarization angles. Reproduced from [76].

scales. Tip-induced near-field effect focuses the laser power to sub-10 nm regime with significantly enhanced laser energy intensity for heating and manufacturing. The previous section presented the principle of temperature measurement by using Raman scattering signal, termed Raman thermometry. Considering this, we combined the tip enhanced near-field effect and the Raman thermometry to achieve the extreme temperature measurement during nanoscale laser manufacturing. As a matter of fact, Raman signal of sub-10 nm regime at the focused area is greatly enhanced due to the enlarged scattering effect [75]. Thus, the Raman thermometry can be regarded as a promising tool for conducting thermophysical studies in extreme manufacturing scenarios.

Figure 3 shows the experimental setup for this tip-induced laser heating and temperature probing. The setup was built based on the AFM platform which precisely controls the tip-substrate distance [75]. It is well known that the tip-substrate distance is important for near-field focusing of laser energy. In the operation, the contact mode of the AFM was set for the tip and substrate interaction since the laser enhancement can achieve the largest level and the maximum enhancement of the Raman signal. A strong Raman signal is critical for successful nanoscale thermal probing. The polarization angle is also important to the near-field enhancement effect. Previously, we validated that changes in the polarization angle of the incident laser can significantly affect optical enhancement [76]. Figure 4 shows the simulation results for electric field distribution around the tip apex for the tip-substrate distance of 6 nm and tip radius of 30 nm. It was found that the enhancement regime was confined within a 10 nm scale and results in figure 4(d) indicate that the enhancement factor rapidly decreased when the polarization angle exceeded 30°.

3.2. *Heating of nano-tip under laser irradiation*

Compared with a continuous laser, a pulsed laser utilizes heat sources that with more intense heating density. However, the heating effect of the tip should be carefully considered because the high energy density of the laser could increase the temperature of the tip. The thermal stress and expansion effect of the

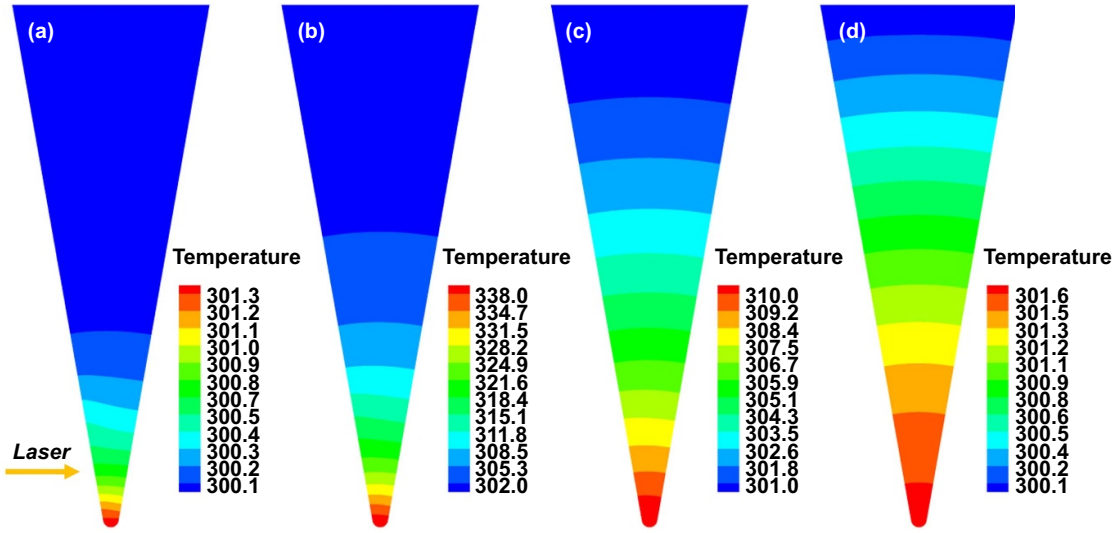

Figure 5. Temperature distribution of the tip at (a) $t = 10$ ns, (b) $t = 20$ ns, (c) $t = 30$ ns, and (d) $t = 40$ ns. Reproduced from [76]. © IOP Publishing Ltd. All rights reserved.

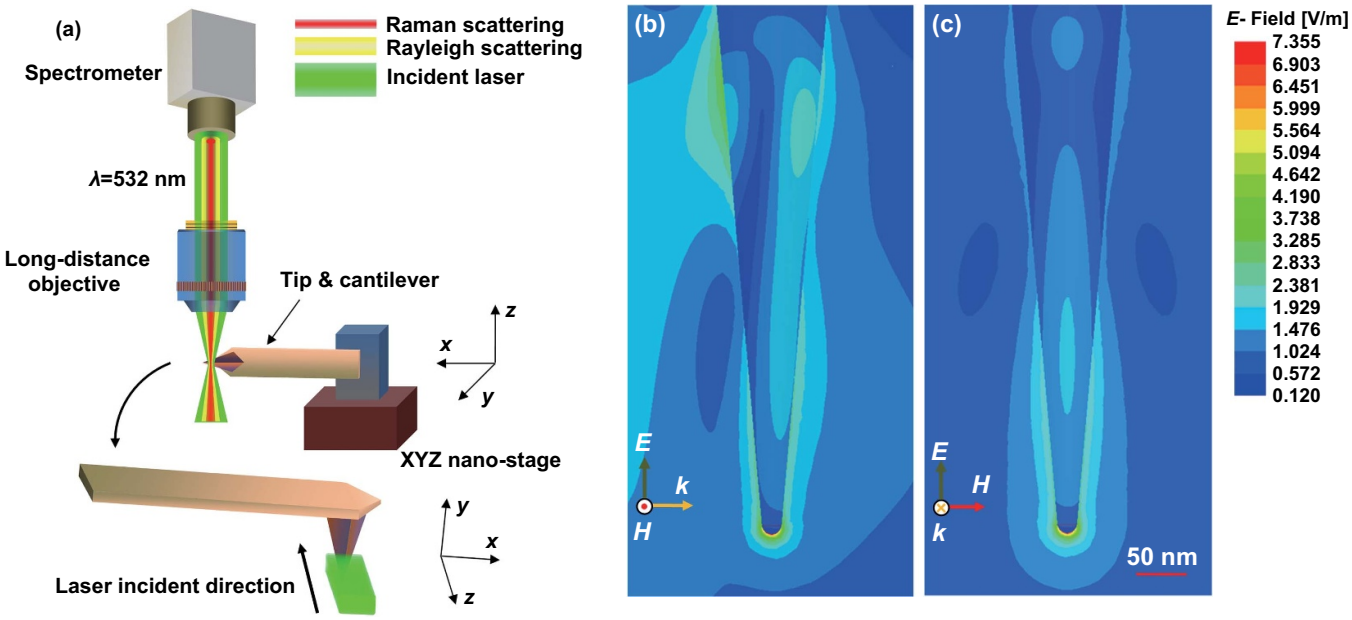

Figure 6. Thermal response of Si nano-tip to laser irradiation: (a) experimental setup for laser heating and Raman probing; (b) front- and (c) side-view of the simulation results of near-field enhancement around the tip. Reprinted with permission from [77]. Copyright (2011) American Chemical Society.

tip, due to large temperature increase, could greatly modify the distance between the tip and substrate and, thus changes the near-field optical enhancement scenario. Chen *et al* studied the temperature rise of the tip under pulsed laser heating (2.5 mJ $\cdot$ cm^{-2}), as shown in figure 5 [76]. As thermal expansion is directly related to the temperature distribution along the tip, the tip apex's temperature should be evaluated with caution.

Raman thermometry is not only effective for studying the tip-substrate interaction, but it is also an effective tool for probing the temperature increase of the tip itself. Most kinds of tips are made of silicon, which has a strong Raman peak at 520 cm^{-1} in the spectrum. During nanotip-induced extreme manufacturing, the temperature rise of the nanotip may result in deformation or even thermal failure. Temperature monitoring could provide an important guide for engineering applications. In 2011, Wang's group reported the experimental observation of temperature rise of silicon nanotip under continuous wave (CW) laser irradiation [77]. As shown in figure 6, they reported that the temperature rise in the tip and cantilever were 754 and 626 K, respectively, under a laser heating density of 5.6 $\times$ 10^8 W $\cdot$ m^{-2}. The substantial temperature

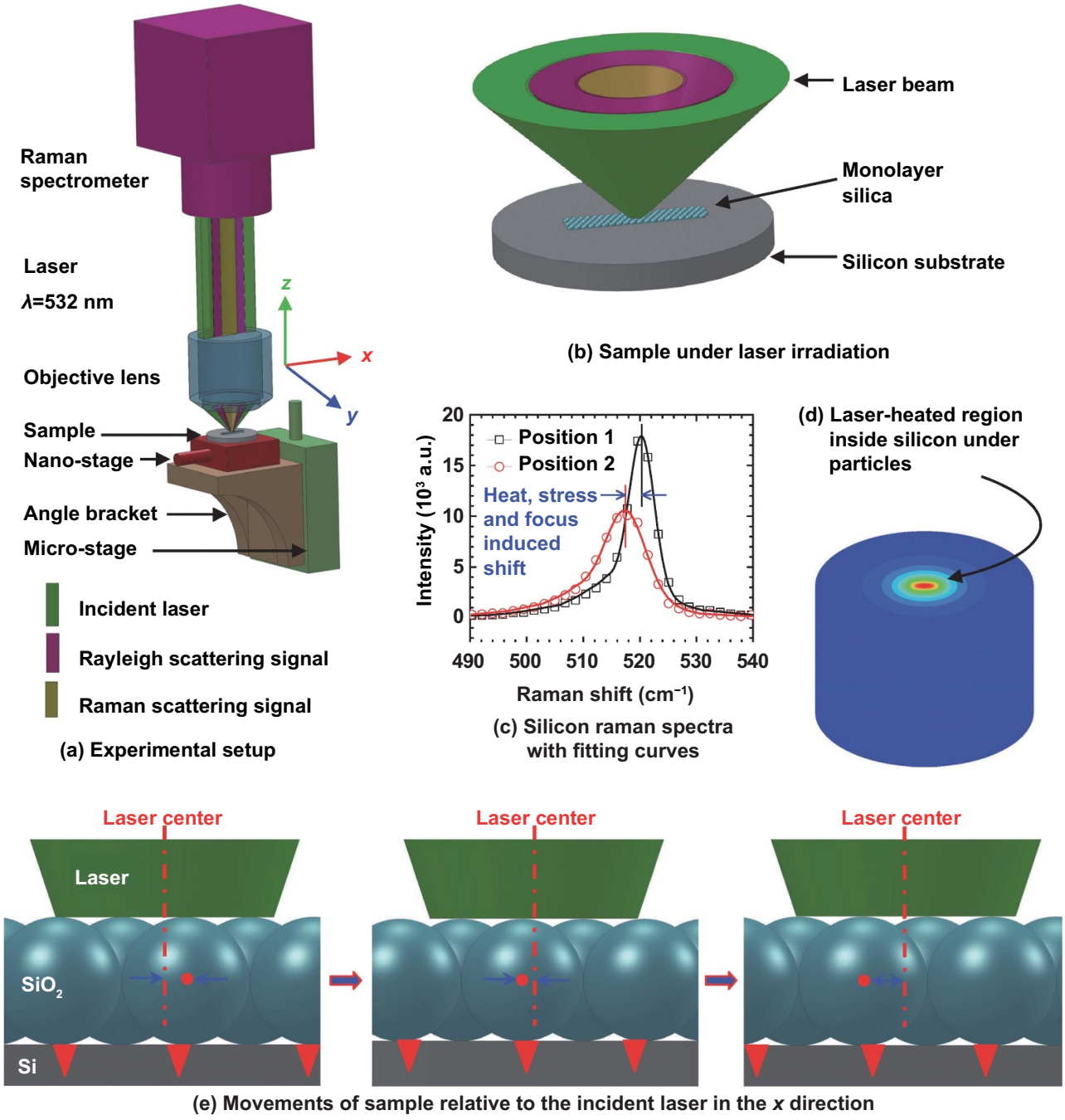

Figure 7. Nanoscale mapping of particle-induced thermal, stress, and optical fields. Reproduced from [81]. CC0 1.0 Universal (CC0 1.0) Public Domain Dedication.

increase was attributed to the optical enhancement around the nanotip and the reduced thermal conductivity of the nanotip due to inefficient phonon transport.

3.3. Near-field optical heating induced by micro/nanoparticles: conjugated physics probing

Besides the nanotip, nanoparticles are also commonly used for inducing near-field optical enhancement. In the biomedical field, gold nanoparticles have been used as the nanoscale heating sources for killing cancer cells based on their plasmonic effect under laser heating [39, 78–80]. Nanoparticles can also be used in imaging instruments to break the diffraction limit combined with Raman scanning. Figure 7 shows the experimental setup for thermal imaging of nanoparticle induced near-field heating. The size of nanoparticle is comparable to or smaller than the wavelength of the laser (e.g. 532 nm) [81]. The geometry of patterned nanoparticles is not observable under a microscope due to the diffraction limit. However, due to the near-field effect generated from the nanoparticle, the enhanced Raman signal from the substrate changes during the Raman scanning process. The Raman

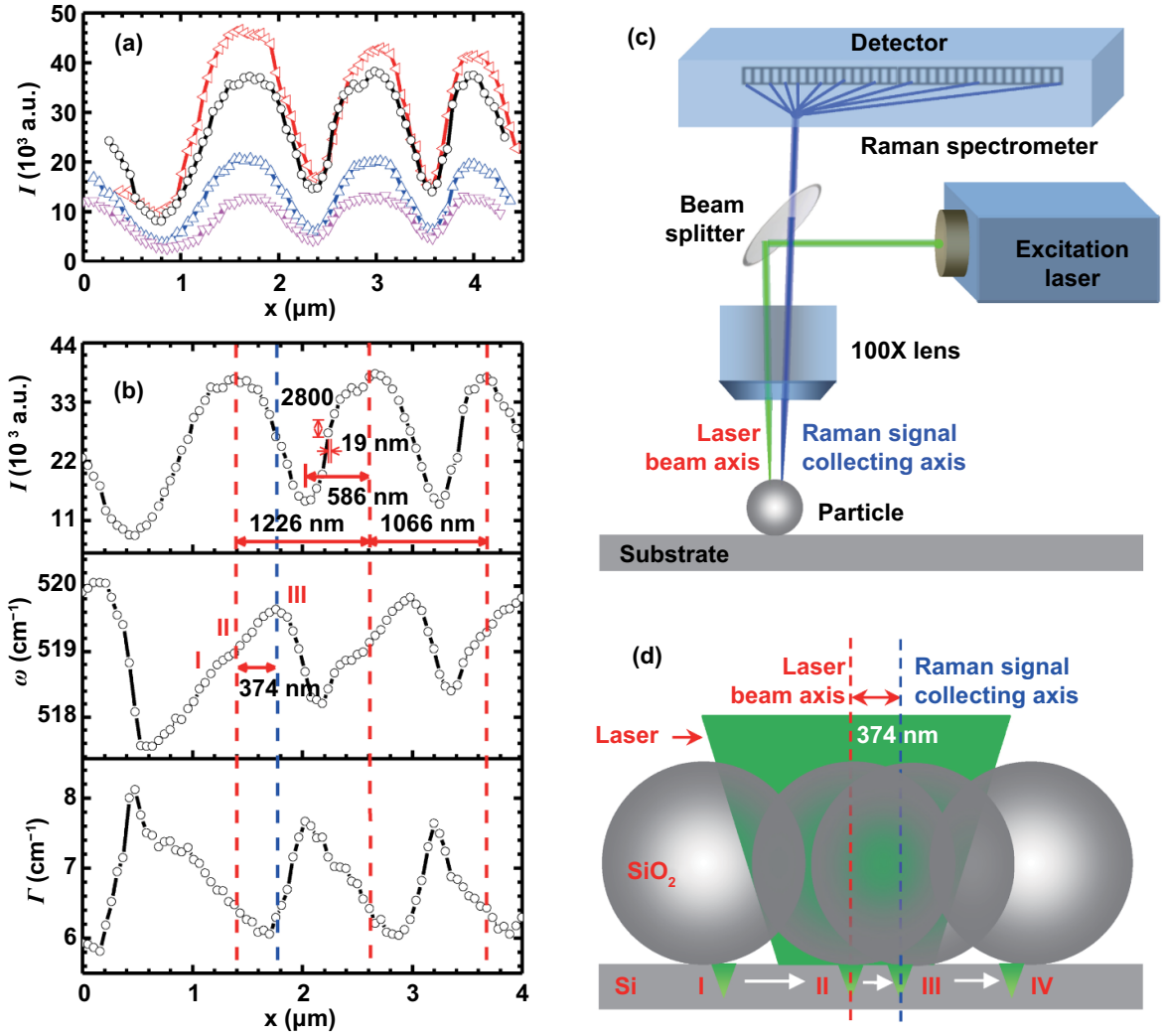

Figure 8. Nanoscale mapping for near-field heating under 1210 nm particles. Reproduced from [81]. CC0 1.0 Universal (CC0 1.0) Public Domain Dedication.

intensity profile shows excellent accordance with the size of nanoparticles. As shown in figure 7, the patterned nanoparticles (silica) were placed on a silicon substrate. A piezo-actuated nano-stage was used to precisely control the movement of the sample. Due to the near-field effect, the region beneath the particle heated up, and the heating effect appeared as a Raman shift of silicon peaks, as shown in figure 7(c). It is known that the Raman spectrum shifts to the left due to laser heating, stress, and the out-of-focus effect. The small heating region (less than 100 mm) makes distinguishing these effects challenging, but doing so is critical to the evaluation of thermophysical process of nanoparticle induced near-field heating.

Raman intensity, linewidth, and Raman shift provide comprehensive information about light-matter interactions, such as stress, temperature rise, and so on. In applications of Raman thermometry, Raman shift properties are widely used for determining the temperature of target materials [49]. However, the shift can result from the strain effect due to stress, which introduces analysis errors. The linewidth is not significantly dependent on temperature, but temperature is a major factor affecting the linewidth. Thus, the Raman shift and linewidth can be used to build the spatial distribution of temperature and stress at the nanoscale [57].

Raman intensity is affected by three factors and can be expressed as $I \sim f_1 f_2 f_3(\Delta T)$, where f_1 denotes the system alignment factor, f_2 represents the intensity change due to laser energy, and $f_3(\Delta T)$ is the intensity variation caused by the temperature. Combined analysis of Raman wavenumber (ω) and linewidth (Γ) was used to determine the thermal stress (σ) inside the substrate. As shown in figure 8, ω decreases and Γ broadens as temperature increases. It is noted that Γ has lower temperature sensitivity than ω and Γ is stress insensitive to the first order, while stress causes a shift in ω. Tang *et al* reported that their mapping results based on Raman intensity variation, wavenumber shift, and linewidth broadening produced consistent conjugated thermal, stress, and near-field focusing effects at a 20 nm resolution [81]. This high spatial resolution was not determined by the wavelength of light sources but by the resolution of the piezo-actuation of the nano-stage. In their work, the Raman intensity difference could be distinguished

over a distance of 20 nm in the sample moving direction, meaning the spatial resolution can reach a similar level.

3.4. Asymmetries during Raman scanning of surface nanostructures

It needs to be noticed that the Raman scanning method is only based on some ideal cases such as very flat/even surface, which means if there is structure variation in space, this structure variation will cause Raman intensity and wavenumber change. Such change cannot be simply taken as temperature and stress effect. Therefore, the structure variation/distribution in space must be taken into serious consideration in scanning Raman for stress and temperature measurements. The asymmetries of Raman scattering along one scanning direction and between two scanning directions should be considered. Such asymmetries are usually caused by the alignment of the detector units in the spectrometer and the pixel numbers along each direction. Wang *et al* discovered that step variation of the sample edge results in a third asymmetry in 2D materials, such as $MoSe_2$ nanosheet, in addition to the asymmetry of Raman shift when scanned along the two directions, a third asymmetry, which was caused by the step variation of the sample edge, was also discovered by Wang *et al* [82]. To address these issues, as shown in figure 9, Wang *et al* reported a data construction method to eliminate these asymmetries [82]. In this method, the Raman signals along the $-x$ and $+x$ directions and the $-y$ and $+y$ directions at the corresponding positions are averaged to eliminate the asymmetries.

4. Raman-based thermal probing: transient response

As mentioned previously, the thermocouple time response is not fast enough to realize the real-time temperature detection of materials under laser heating. Infrared thermometry technique is hard to measure the transient response of samples under ultrafast laser pulse heating or for nanoscale regions.

The pump-probe thermoreflectance technique is an optical technique that can be used to measure heat transfer in bulk materials and micro/nanoscale samples. In this technique, two lasers are used as the pump and probe. The pump beam irradiates the sample to generate a time-dependent heat flux, while the probe beam is used to characterize the temperature response through a proportional change in surface reflectivity. Then, the thermal properties, which include the cross-plane and in-plane thermal conductivities, heat capacity, and thermal boundary conductance between materials, can be determined by combining with a heat transfer model [83]. Though pump-probe thermoreflectance can probe the material's thermal response, a thin layer of metal is usually needed to coat the samples, especially for samples with rough surfaces. This metal layer—which is opaque at both pump and probe wavelengths and has a large thermoreflectance coefficient at the probe wavelength—is used as a transducer layer. The technique provides a relative measurement method, which indicates that the accuracy will be lower. This technique cannot be used in situations with extremely high temperatures.

Raman spectroscopy can also be used for fast or ultrafast thermal response probing, which is critical for understanding the transient thermal response of materials in laser extreme manufacturing. One way is to use a single pulsed laser for both laser heating and Raman signal excitation. Wang's group developed a technique called energy transport state resolved Raman (ET-Raman) for probing thermal transport in 2D materials. In this technique, different energy transport states in both space and time domains are constructed to probe a materials' thermal response in different situations [62, 84–86]. As shown in figure 10, three physical processes take place during laser heating: hot carrier generation, diffusion in space, and electron-hole recombination. All three processes affect the sample's thermal response. This process, which involves heat transfer and energy redistribution, is determined by the hot carrier diffusivity. Subsequently, phonons, which receive energy from hot carriers or electron-hole recombination, conduct heat in 2D materials. This heat conduction is mainly related to the in-plane thermal conductivity of a 2D material. Finally, the heat is conducted from the 2D material to the substrate, and this process is dominated by the local thermal resistance. The novel five-state ET-Raman method takes into consideration the critical effects of hot carrier diffusion, electron-hole recombination, and energy coupling with phonons when determining the thermal conductivity of supported 2D materials for the first time [62]. Although this work focuses on supported 2D materials, the thermal transport of suspended 2D materials can also be explored by using the ET-Raman method. Certain substrates, such as silicon, for supported samples, show extremely high thermal conductivity, which indicates that the thermal transport will quickly reach steady state. As a result, a picosecond laser is used to construct the transient energy transport state. However, this picosecond laser cannot be used for suspended samples because the short pulse interval may cause a heat accumulation effect that could destroy the sample. A nanosecond laser can be used instead [85, 86]. Although the ET-Raman technique is primarily used to study thermal transport, it provides a novel way of probing a material's thermal response under ultrafast laser heating.

Raman pump-probe spectroscopy can be an alternative technique. This technique also uses two pulsed lasers: one laser for designated laser heating and manufacturing, and another laser for Raman excitation. The time delay of the two lasers can be adjusted using the same manner in the pump-probe technique. In this technique, a strong pump pulse is focused onto the sample to create a time-dependent heat flux, while a weak time-delayed probe pulse monitors the response of the surface temperature through Raman transitions [87].

For many laser extreme manufacturing situations, the temperature could be very high, which makes the Raman signal extremely low. Two special Raman techniques: stimulated Raman scattering (SRS) and coherent anti-Stokes Raman scattering (CARS), can significantly enhance the Raman signal. SRS is a coherent Raman scattering technique that generates signals by the co-alignment of two incident beams (i.e. the pump and Stokes beams), as shown in figure 11. Tuning the frequency difference between the two beams to match a

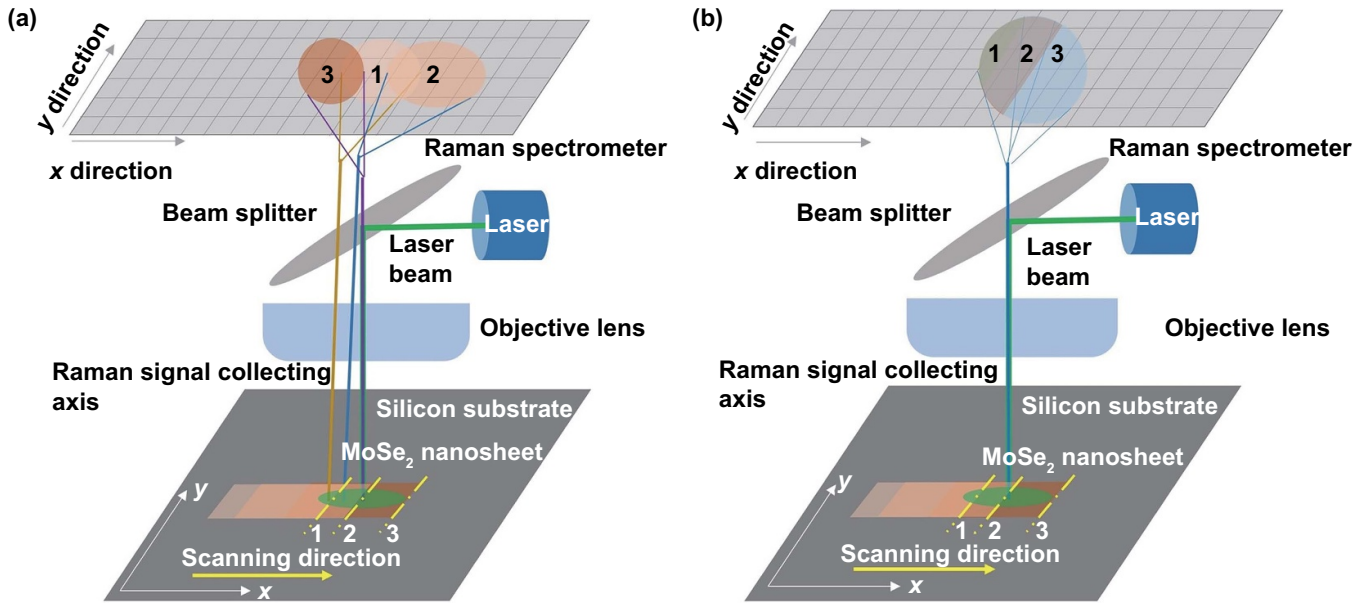

Figure 9. Schematic of the scanning Raman system used to detect the Raman signal of (a) silicon substrate and (b) $MoSe_2$ nanosheet. Reproduced with permission from [82]. © 2017 Optical Society of America.

molecular vibration stimulates Raman active molecular vibration. As a result of the coherent excitation of a molecular vibration, the sample absorbs a pump photon and generates a Stokes photon, resulting in stimulated Raman loss (SRL) and stimulated Raman gain (SRG), respectively. These two signals are proportional to the number of molecules in the probe volume and the molecular Raman scattering cross-section. Because the vibrational modes are prepared in a coherent fashion, they oscillate in unison to form a coherent polarization in the sample. The subsequent radiation derived from the polarization is also coherent. The resulting SRS radiation is strong and highly directional, enhancing vibrational excitation by a factor of 10^7, offering signal detection efficiencies that are many orders of magnitude higher than spontaneous Raman scattering. Additionally, the SRS technique enables direct observation of the coherent molecular motions at ultrafast time scales, following their evolution and dephasing as a function of time. This allows for a time-resolved view of processes and molecular dynamics that cannot always by directly inferred from an analysis of the Raman spectra alone. SRS is also used to measure the temperature of condensed matter at the molecular vibrational level [88].

CARS is another method of enhancing the Raman signal. This method is a nonlinear variant of Raman spectroscopy, which combines signal enhancement by more than four orders of magnitude with further advantages such as directional emission, and narrow spectral bandwidth [89–91]. CARS consists of two stimulated Raman scattering steps. First, a pump photon with a frequency of ω_p and a Stokes photon with a frequency of ω_s resonantly excite a Raman oscillator with a vibrational frequency of $\Omega = \omega_p - \omega_s$. Then, the Raman oscillator is de-excited by a probe photon with a frequency of ω_{pr} to produce an anti-Stokes photon with a frequency of $\omega_{as} = \omega_{pr} + \Omega$. An energy diagram and molecular illustration of the CARS process are shown in figure 12 [92]. An important advantage of CARS over spontaneous Raman scattering is that background fluorescence from the samples does not interfere with the CARS signal detection. Because of the coherent property, the CARS signal increases quadratically with respect to the number of vibrational oscillators in the focal volume. This technique has been used widely to obtain gas-phase temperature because of its high accuracy, precision, relative insensitivity to the collisional environment, and because it can be applied even in high luminous flames [93].

5. Concluding remarks and outlook

As all the LAM processes involve intensive heating, it is crucial to probe the materials' thermal response to understand the physics behind these processes, including laser absorption, heating, heat conduction, melting, vaporization, and crystallization/solidification. Raman spectroscopy offers a novel way of measuring temperature during laser-assisted extreme manufacturing. In this review, the basic mechanisms of Raman-based temperature probing were introduced. Various Raman-based techniques used for temperature probing, including near-field Raman thermometry, ET-Raman, pump-probe Raman technique, SRS method, and CARS method were critically reviewed for their measurement mechanism as well as their applications.

In laser-assisted extreme manufacturing, extreme stress usually accompanies significantly elevated temperatures. As a result, extreme caution must be taken when using Raman wavenumber for temperature measurement as it can be strongly affected by local stress. Combined use of Raman wavenumber and linewidth is highly recommended to distinguish and measure both temperature and stress. In spontaneous Raman spectroscopy, the focal level and surface morphology/structure (even at the scale of tens of nm)

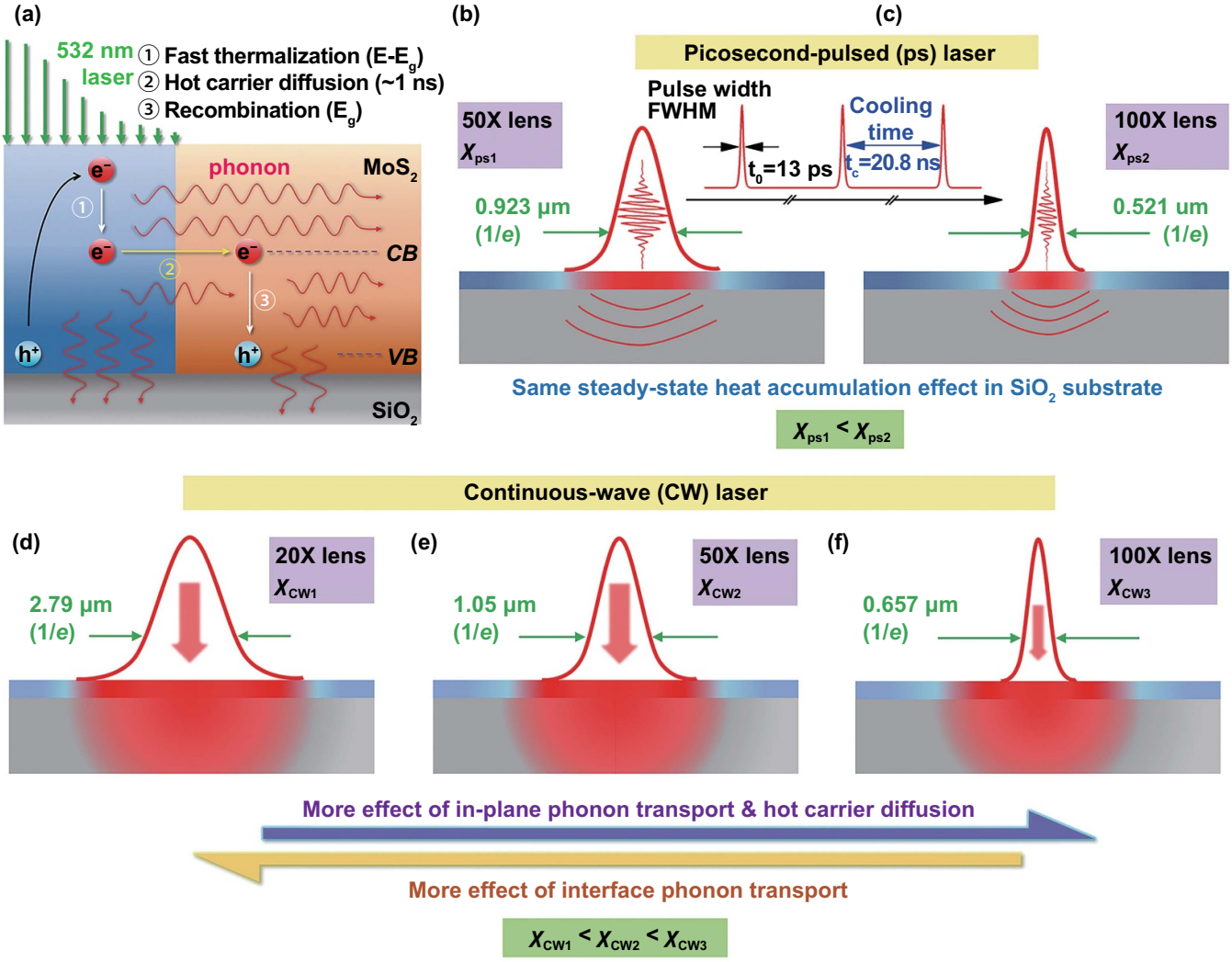

Figure 10. The schematic for the physical principle of five-state picosecond ET-Raman technique. (a) The generation, diffusion of hot carrier, and electron-hole recombination. (b), (c) Two sub-states in ps laser heating under 50× and 100× objective lenses. (d)–(f) Three sub-states in CW laser heating under 20×, 50×, and 100× objective lenses. Reproduced from [62] with permission of The Royal Society of Chemistry.

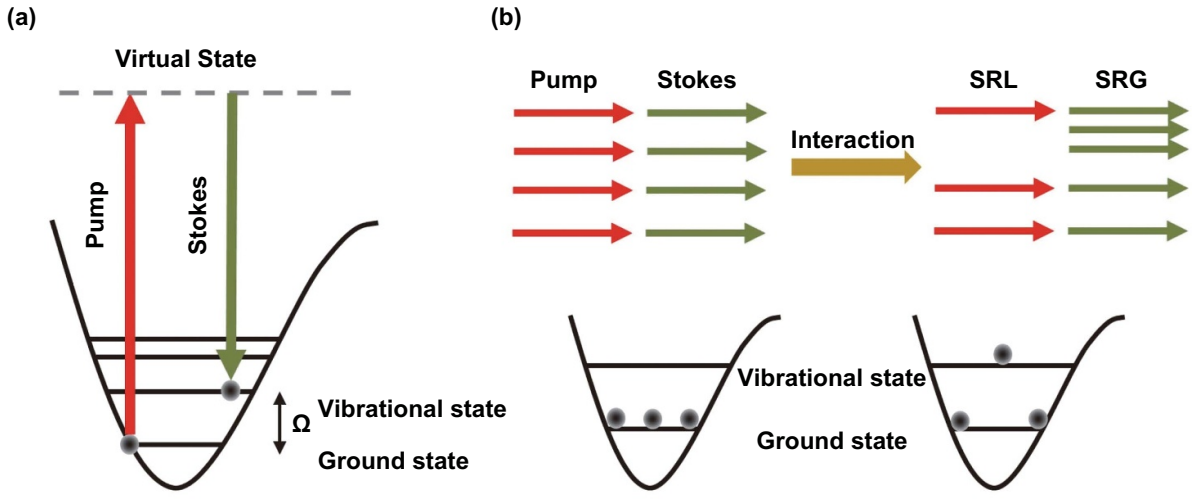

Figure 11. Principle of stimulated Raman scattering. (a) Energy diagram of SRS. (b) Output spectrum associated with SRS process.

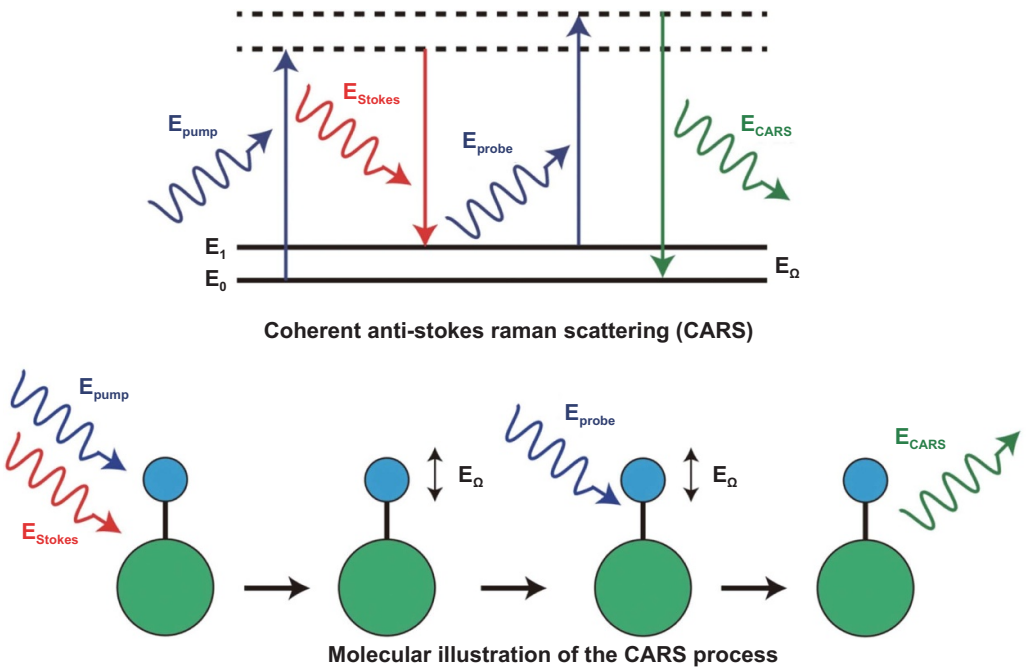

Figure 12. Energy diagram and molecular illustration of the CARS process. Reproduced with permission from [92]. © 2011 Molecular Vision.

can alter the optical path of the Raman signal back to the detector, and induce undesired changes in Raman properties. This type of surface-induced change is sometimes embedded in the temperature-induced Raman properties change and should be carefully considered to obtain physically reasonable information on local temperature rise.

In some LAM processes, for instance laser peening and laser nanoimprinting, there are few methods of characterizing the temperature of the target during the manufacturing process because of the nanoscale geometry as well as the high heating density. Raman thermometry can be used in such scenario, not just because of its non-contact nature but also its enhanced signal due to the near-field effect. Many LAM processes, such as laser-assisted cutting, laser peening, etc, can reach extremely high temperatures, resulting in weak Raman signals. SRS and CARS could dramatically enhance the Raman signal to realize temperature probing in such manufacturing processes. Raman spectra can also be used to characterize the structure variation of a sample, which makes Raman-based techniques suitable candidates for characterization of structure variation of materials during manufacturing processes.

In laser-assisted extreme manufacturing, if the target material is not Raman active (e.g. metals), a Raman active material can be placed in the manufacturing region for temperature probing. For instance, high temperature-resistant materials, such as diamond nanoparticles and graphene, can be used for very efficient Raman signal excitation and ultrafast probing due to the sensor's extremely low thermal inertia. It should be noted that even without near-field focusing, the temperature probing resolution can still exceed the diffraction limit by using nanoscale Raman sensing materials/structures whose feature sizes are significantly smaller than the focal spot.

Additionally, in many LAM processes, temperature variation occurs extremely quickly in material (within picoseconds in some cases). In such situations, Raman techniques with a picosecond/femtosecond pulsed laser can be used to explore the transient thermal response of materials and the possible structure variation during such short heating process. This technique can also realize a high spatial resolution because the laser spot size is controllable. As a result, the Raman technique is a promising method for probing the thermal response of materials with high resolution in time and space domains.

Acknowledgments

We are grateful for the financial support of National Key R&D Program of China (Nos. 2018YFE0205000 and 2019YFA0905800 for R W), Program for Professor of Special Appointment (Eastern Scholar) at Shanghai Institutions of Higher Learning and China Scholarship Council (S X), National Natural Science Foundation of China (No. 5157614 for Y Y) and US National Science Foundation (CBET1930866 for X W).

ORCID iD

Xinwei Wang https://orcid.org/0000-0002-9373-3750

References

[1] Kim K S, Kim J H, Choi J Y and Lee C M 2011 A review on research and development of laser assisted turning *Int. J. Precis. Eng. Manuf.* **12** 753–9
[2] Dutta Majumdar J and Manna I 2011 Laser material processing *Int. Mater. Rev.* **56** 341–88

[3] Zhao L J, Cheng J, Chen M J, Yuan X D, Liao W, Liu Q, Yang H and Wang H J 2019 Formation mechanism of a smooth, defect-free surface of fused silica optics using rapid CO_2 laser polishing *Int. J. Extrem. Manuf.* **1** 035001

[4] Cvecek K, Dehmel S, Miyamoto I and Schmidt M 2019 A review on glass welding by ultra-short laser pulses *Int. J. Extrem. Manuf.* **1** 042001

[5] Gautam G D and Pandey A K 2018 Pulsed Nd: yAGlaser beam drilling: a review *Opt. Laser Technol.* **100** 183–215

[6] Dewil R, Vansteenwegen P and Cattrysse D 2016 A review of cutting path algorithms for laser cutters *Int. J. Adv. Manuf. Technol.* **87** 1865–84

[7] Yocom C J, Zhang X and Liao Y L 2018 Research and development status of laser peen forming: a review *Opt. Laser Technol.* **108** 32–45

[8] Barner-Kowollik C, Bastmeyer M, Blasco E, Delaittre G, Müller P, Richter B and Wegener M 2017 3D laser micro- and nanoprinting: challenges for chemistry *Angew. Chem. Int. Ed.* **56** 15828–45

[9] Gu D D, Meiners W, Wissenbach K and Poprawe R 2012 Laser additive manufacturing of metallic components: materials, processes and mechanisms *Int. Mater. Rev.* **57** 133–64

[10] Chimmalgi A, Grigoropoulos C P and Komvopoulos K 2005 Surface nanostructuring by nano-/femtosecond laser-assisted scanning force microscopy *J. Appl. Phys.* **97** 104319

[11] Meijer J 2004 Laser beam machining (LBM), state of the art and new opportunities *J. Mater. Process. Technol.* **149** 2–17

[12] Dubey A K and Yadava V 2008 Laser beam machining—A review *Int. J. Mach. Tools Manuf.* **48** 609–28

[13] Arrizubieta J I, Klocke F, Gräfe S, Arntz K and Lamikiz A 2015 Thermal simulation of laser-assisted turning *Proced. Eng.* **132** 639–46

[14] Dhakal B and Swaroop S 2018 Review: laser shock peening as post welding treatment technique *J. Manuf. Process.* **32** 721–33

[15] Gujba A K and Medraj M 2014 Laser peening process and its impact on materials properties in comparison with shot peening and ultrasonic impact peening *Materials (Basel)* **7** 7925–74

[16] Montross C S, Wei T, Ye L, Clark G and Mai Y W 2002 Laser shock processing and its effects on microstructure and properties of metal alloys: a review *Int. J. Fatigue* **24** 1021–36

[17] Zhang X C, Zhang Y K, Lu J Z, Xuan F Z, Wang Z D and Tu S T 2010 Improvement of fatigue life of Ti–6Al–4V alloy by laser shock peening *Mater. Sci. Eng.* A **527** 3411–5

[18] Hsiao F B, Jen C P, Wang D B, Chuang C H, Lee Y C, Liu C P and Hsu H J 2006 An analytical modeling of heat transfer for laser-assisted nanoimprinting processes *Comput. Mech.* **37** 173–81

[19] Ahmadi Z, Yakupoglu B, Azam N, Elafandi S and Mahjouri-Samani M 2019 Self-limiting laser crystallization and direct writing of 2D materials *Int. J. Extrem. Manuf.* **1** 015001

[20] Li L P, Lu Y F, Doerr D W, Alexander D R, Shi J and Li J C 2004 Fabrication of hemispherical cavity arrays on silicon substrates using laser-assisted nanoimprinting of self-assembled particles *Nanotechnology* **15** 333–6

[21] Wu G Q, Hu Y Z, Zhu W N, Song C G and Han H S 2017 Research status and development trend of laser additive manufacturing technology *Proc. 4th Int. Conf. on Information Science and Control Engineering* (Changsha, China: IEEE) pp 1210–3

[22] Melchels F P W, Domingos M A N, Klein T J, Malda J, Bartolo P J and Hutmacher D W 2012 Additive manufacturing of tissues and organs *Prog. Polym. Sci.* **37** 1079–104

[23] Buchbinder D, Schleifenbaum H, Heidrich S, Meiners W and Bültmann J 2011 High power selective laser melting (HP SLM) of aluminum parts *Phys. Procedia* **12** 271–8

[24] Baufeld B, van der Biest O and Gault R 2010 Additive manufacturing of Ti–6Al–4V components by shaped metal deposition: microstructure and mechanical properties *Mater. Des.* **31** S106–11

[25] Murr L E, Martinez E, Amato K N, Gaytan S M, Hernandez J, Ramirez D A, Shindo P W, Medina F and Wicker R B 2012 Fabrication of metal and alloy components by additive manufacturing: examples of 3D materials science *J. Mater. Res. Technol.* **1** 42–54

[26] Wang X W 2005 Large-scale molecular dynamics simulation of surface nanostructuring with a laser-assisted scanning tunnelling microscope *J. Phys. D: Appl. Phys.* **38** 1805–23

[27] Jersch J, Demming F and Dickmann K 1996 Nanostructuring with laser radiation in the nearfield of a tip from a scanning force microscope *Appl. Phys.* A **64** 29–32

[28] Xu S, Zhang L J, Yue Y N and Wang X W 2015 Physics in laser near-field nanomanufacturing: fundamental understanding and novel probing *Encyclopedia of Nanotechnology* ed B Bhushan (Dordrecht: Springer) pp 3195–213

[29] Mai Z H, Lu Y F, Huang S M, Chim W K and Pan J S 2000 Mechanism of laser-induced nanomodification on hydrogen-passivated Si(100) surfaces underneath the tip of a scanning tunneling microscope *J. Vac. Sci. Technol.* B **18** 1853–7

[30] Mai Z H, Lu Y F, Song W D and Chim W K 2000 Nano-modification on hydrogen-passivated Si surfaces by a laser-assisted scanning tunneling microscope operating in air *Appl. Surf. Sci.* **154–5** 360–4

[31] Kim M M, Giry A, Mastiani M, Rodrigues G O, Reis A and Mandin P 2015 Microscale thermometry: a review *Microelectron. Eng.* **148** 129–42

[32] Hetsroni G, Mosyak A, Pogrebnyak E and Rozenblit R 2011 Infrared temperature measurements in micro-channels and micro-fluid systems *Int. J. Therm. Sci.* **50** 853–68

[33] Astarita T, Cardone G, Carlomagno G M and Meola C 2000 A survey on infrared thermography for convective heat transfer measurements *Opt. Laser Technol.* **32** 593–610

[34] Tian B, Zhang Z K, Shi P, Zheng C, Yu Q Y, Jing W X and Jiang Z D 2017 Tungsten-rhenium thin film thermocouples for SiC-based ceramic matrix composites *Rev. Sci. Instrum.* **88** 015007

[35] Kölbl N, Marschall I and Harmuth H 2019 High-temperature investigation of mould slag crystallization by single and double hot thermocouple techniques *J. Iron Steel Res. Int.* **26** 345–54

[36] Tougas M I, Amani M and Gregory O J 2013 Metallic and ceramic thin film thermocouples for gas turbine engines *Sensors* **13** 15324–47

[37] Sonibare O O, Haeger T and Foley S F 2010 Structural characterization of nigerian coals by X-ray diffraction, raman and FTIR spectroscopy *Energy* **35** 5347–53

[38] He X Q, Liu X F, Nie B S and Song D Z 2017 FTIR and Raman spectroscopy characterization of functional groups in various rank coals *Fuel* **206** 555–63

[39] Yue Y N and Wang X W 2012 Nanoscale thermal probing *Nano Rev.* **3** 11586

[40] Xu S, Wang T Y, Hurley D, Yue Y N and Wang X W 2015 Development of time-domain differential Raman for transient thermal probing of materials *Opt. Express* **23** 10040–56

[41] Serrano J R, Phinney L M and Kearney S P 2006 Micro-Raman thermometry of thermal flexure actuators *J. Micromech. Microeng.* **16** 1128–34

[42] Kittel C 2004 *Introduction to Solid State Physics* (New York: Wiley)

[43] Attal-Trétout B, Bouchardy P, Magre P, Péalat M and Taran J P 1990 CARS in combustion: prospects and problems *Appl. Phys.* B **51** 17–24

[44] Harris D C and Bertolucci M D 1978 *Symmetry and Spectroscopy: An Introduction to Vibrational and Electronic Spectroscopy* (Oxford: Oxford University Press)

[45] Cialla-May D, Schmitt M and Popp J 2019 Theoretical principles of Raman spectroscopy *Phys. Sci. Rev.* **4** 20170040

[46] Das R S and Agrawal Y K 2011 Raman spectroscopy: recent advancements, techniques and applications *Vib. Spectrosc.* **57** 163–76

[47] Childs P R N, Greenwood J R and Long C A 2000 Review of temperature measurement *Rev. Sci. Instrum.* **71** 2959–78

[48] Xu Z W, He Z D, Song Y, Fu X, Rommel M, Luo X C, Hartmaier A, Zhang J J and Fang F Z 2018 Topic review: application of raman spectroscopy characterization in micro/nano-machining *Micromachines* **9** 361

[49] Yue Y N, Zhang J C and Wang X W 2011 Micro/nanoscale spatial resolution temperature probing for the interfacial thermal characterization of epitaxial graphene on 4H-SiC *Small* **7** 3324–33

[50] Wallis R F and Balkanski M 1986 *Many-Body Aspects of Solid State Spectroscopy* (Amsterdam: North-Holland)

[51] Weber W H and Merlin R 2000 *Raman Scattering in Materials Science* (Berlin: Springer)

[52] Hosoya N, Akaho Y, Inoue M, Sahoo S and Tachibana M 2014 Temperature dependence of the Raman spectra of polycrystalline graphene grown by chemical vapor deposition *Appl. Phys. Lett.* **105** 023108

[53] Huang X T, Gao Y, Yang T Q, Ren W C, Cheng H M and Lai T S 2016 Quantitative analysis of temperature dependence of Raman shift of monolayer WS_2 *Sci. Rep.* **6** 32236

[54] Hart T R, Aggarwal R L and Lax B 1970 Temperature dependence of Raman scattering in silicon *Phys. Rev.* B **1** 638–42

[55] John N and George S 2017 Raman spectroscopy *Spectroscopic Methods for Nanomaterials Characterization*, ed S Thomas, R Thomas, A K Zachariah and R K Mishra (Amsterdam: Elsevier) pp 95–127

[56] Sun H Y, Xu Z and Gao C 2013 Multifunctional, ultra-flyweight, synergistically assembled carbon aerogels *Adv. Mater.* **25** 2554–60

[57] Tang X D, Xu S and Wang X W 2013 Thermal probing in single microparticle and microfiber induced near-field laser focusing *Opt. Express* **21** 14303–15

[58] Wang Z L and Tang D W 2013 Investigation of heat transfer around microwire in air environment using 3ω method *Int. J. Therm. Sci.* **64** 145–51

[59] Rumble J R 2019 *CRC Handbook of Chemistry and Physics* 100th edn (Boca Raton, FL: CRC Press)

[60] Yuan P Y, Li C, Xu S, Liu J and Wang X W 2017 Interfacial thermal conductance between few to tens of layered-MoS_2 and c-Si: effect of MoS_2 thickness *Acta Mater.* **122** 152–65

[61] Yuan P Y, Liu J, Wang R D and Wang X W 2017 The hot carrier diffusion coefficient of sub-10 nm virgin MoS_2: uncovered by non-contact optical probing *Nanoscale* **9** 6808–20

[62] Yuan P Y, Wang R D, Wang T Y, Wang X W and Xie Y S 2018 Nonmonotonic thickness-dependence of in-plane thermal conductivity of few-layered MoS_2: 2.4 to 37.8 nm *Phys. Chem. Chem. Phys.* **20** 25752–61

[63] Tang X D, Xu S and Wang X W 2014 Corrugated epitaxial graphene/SiC interfaces: photon excitation and probing *Nanoscale* **6** 8822–30

[64] van de Burgt Y 2014 Laser-assisted growth of carbon nanotubes—A review *J. Laser Appl.* **26** 032001

[65] Tofail S A M, Koumoulos E P, Bandyopadhyay A, Bose S, O'Donoghue L and Charitidis C 2018 Additive manufacturing: scientific and technological challenges, market uptake and opportunities *Mater. Today* **21** 22–37

[66] Tang X D, Xu S, Zhang J C and Wang X W 2014 Five orders of magnitude reduction in energy coupling across corrugated graphene/substrate interfaces *ACS Appl. Mater. Interfaces* **6** 2809–18

[67] Zhou H Q, Qiu C Y, Yu F, Yang H C, Chen M J, Hu L J, Guo Y J and Sun L F 2011 Raman scattering of monolayer graphene: the temperature and oxygen doping effects *J. Phys. D: Appl. Phys.* **44** 185404

[68] Zhang L, Jia Z, Huang L M, O'Brien S and Yu Z H 2008 Low-temperature raman spectroscopy of individual single-wall carbon nanotubes and single-layer graphene *J. Phys. Chem.* C **112** 13893–900

[69] Allen M J, Fowler J D, Tung V C, Yang Y, Weiller B H and Kaner R B 2008 Temperature dependent Raman spectroscopy of chemically derived graphene *Appl. Phys. Lett.* **93** 193119

[70] Calizo I, Balandin A A, Bao W, Miao F and Lau C N 2007 Temperature dependence of the raman spectra of graphene and graphene multilayers *Nano Lett.* **7** 2645–9

[71] Balandin A A 2011 Thermal properties of graphene and nanostructured carbon materials *Nat. Mater.* **10** 569–81

[72] Zhao W Q, Chen W, Yue Y N and Wu S J 2017 In-situ two-step Raman thermometry for thermal characterization of monolayer graphene interface material *Appl. Therm. Eng.* **113** 481–9

[73] Wang W H, Peng Q, Dai Y Q, Qian Z F and Liu S 2016 Temperature dependence of Raman spectra of graphene on copper foil substrate *J. Mater. Sci. Mater. Electron.* **27** 3888–93

[74] Malard L M, Nilsson J, Mafra D L, Elias D C, Brant J C, Plentz F, Alves E S, Neto A H C and Pimenta M A 2008 Electronic properties of bilayer graphene probed by resonance Raman scattering *Phys. Status Solidi* b **245** 2060–3

[75] Yue Y N, Chen X W and Wang X W 2011 Noncontact sub-10 nm temperature measurement in near-field laser heating *ACS Nano* **5** 4466–75

[76] Chen X W and Wang X W 2011 Near-field thermal transport in a nanotip under laser irradiation *Nanotechnology* **22** 075204

[77] Chen X W and Wang X W 2011 Microscale spatially resolved thermal response of Si nanotip to laser irradiation *J. Phys. Chem.* C **115** 22207–16

[78] Kucsko G, Maurer P C, Yao N Y, Kubo M, Noh H J, Lo P K, Park H and Lukin M D 2013 Nanometre-scale thermometry in a living cell *Nature* **500** 54–58

[79] Li C Z and Yue Y N 2014 Fluorescence spectroscopy of graphene quantum dots: temperature effect at different excitation wavelengths *Nanotechnology* **25** 435703

[80] Neumann P *et al* 2013 High-precision nanoscale temperature sensing using single defects in diamond *Nano Lett.* **13** 2738–42

[81] Tang X D, Xu S and Wang X W 2013 Nanoscale probing of thermal, stress, and optical fields under near-field Laser heating *PLoS One* **8** e58030

[82] Wang R D, Yuan P Y, Han M, Xu S, Wang T Y and Wang X W 2017 Asymmetry of Raman scattering by structure variation in space *Opt. Express* **25** 18378–92

[83] Schmidt A J 2013 Pump-probe thermoreflectance *Annu. Rev. Heat Transf.* **16** 159–81

[84] Yuan P Y, Wang R D, Tan H, Wang T Y and Wang X W 2017 Energy transport state resolved raman for probing interface energy transport and hot carrier diffusion in few-layered MoS_2 *ACS Photonics* **4** 3115–29

[85] Wang R D, Wang T Y, Zobeiri H, Yuan P Y, Deng C, Yue Y N, Xu S and Wang X W 2018 Measurement of the thermal conductivities of suspended MoS_2 and $MoSe_2$ by

nanosecond ET-Raman without temperature calibration and laser absorption evaluation *Nanoscale* **10** 23087–102
[86] Zobeiri H, Wang R D, Zhang Q Y, Zhu G J and Wang X W 2019 Hot carrier transfer and phonon transport in suspended nm WS_2 films *Acta Mater.* **175** 222–37
[87] Souther N, Wagner R, Harnish P, Briel M and Bali S 2010 Measurements of light shifts in cold atoms using Raman pump-probe spectroscopy *Laser Phys. Lett.* **7** 321–7
[88] Dang N C, Bolme C A, Moore D S and McGrane S D 2011 Femtosecond stimulated raman scattering picosecond molecular thermometry in condensed phases *Phys. Rev. Lett.* **107** 043001
[89] Müller M and Zumbusch A 2007 Coherent anti-Stokes Raman scattering microscopy *ChemPhysChem* **8** 2156–70
[90] Krafft C, Dietzek B and Raman P J 2009 CARSmicrospectroscopy of cells and tissues *Analyst* **134** 1046–57
[91] Tu H H and Boppart S A 2014 Coherent anti-Stokes Raman scattering microscopy: overcoming technical barriers for clinical translation *J. Biophoton.* **7** 9–22
[92] Lei T C, Ammar D A, Masihzadeh O, Gibson E A and Kahook M Y 2011 Label-free imaging of trabecular meshwork cells using coherent anti-Stokes Raman scattering (CARS) microscopy *Mol. Vis.* **17** 2628–33
[93] Dennis C N, Satija A and Lucht R P 2016 High dynamic range thermometry at 5 kHz in hydrogen–air diffusion flame using chirped-probe-pulse femtosecond coherent anti-Stokes Raman scattering *J. Raman Spectrosc.* **47** 177–88